JOURNAL OF GEOPHYSICAL RESEARCH, VOL. 92, NO. A5, PAGES 4649-4662, MAY 1, 1987

MSIS-86 THERMOSPHERIC MODEL

Alan E. Hedin

Planetary Atmospheres Branch, NASA Goddard Space Flight Center, Greenbelt, Maryland

Abstract. The MSIS-86 empirical model of thermospheric temperature, density and composition uses new temperature and composition data from the Dynamics Explorer satellite to improve the representation of polar region morphology over that in the MSIS-83 model. Terms were added or changed to better represent seasonal variations in the polar regions under both quiet and magnetically disturbed conditions. Local time variations in the magnetic activity effect were added. In addition a new species, atomic nitrogen, was added to the previous list of N_2, O_2, He, O, H, and Ar covered by the model.

1. Introduction

The MSIS-83 empirical model [Hedin, 1983] of thermospheric temperature and density, based on in situ data from seven satellites and numerous rocket probes, as well as five ground based incoherent scatter stations, provided predictions of temperature and densities for N_2, O_2, O, He, Ar, and H. Recently, the in situ temperature and composition measurements from the Dynamics Explorer B satellite have become available, providing good coverage of the polar regions just after the peak of solar cycle 21. These DE-B data [Hedin and Carignan, 1985] suggested several refinements in the description of polar region morphology, especially in regard to seasonal differences. Atomic nitrogen has been added to the list of species included in the model based on data from Atmospheric Explorer C, D, and E and Dynamics Explorer B. Individual models for the atomic nitrogen data from AE-C and AE-E have been described by Engebretson et al. [1977] and Engebretson et al. [1980]. Several additional years of temperature data from St. Santin were also used in generating the model.

This paper presents and discusses the 1986 MSIS model with some indication of differences from the previous models.

2. Model Formulation

The model formulation (see appendix for details) has been discussed in detail by Hedin [1983]. The model uses a Bates temperature profile as a function of geopotential height for the upper thermosphere and an inverse polynomial in geopotential height for the lower thermosphere. Exospheric temperature and other key quantities are expressed as functions of geographical and solar/magnetic parameters. These temperature profiles allow exact integration of the hydrostatic equation for a constant mass to determine a density profile based on a density specified at 120 km as a function of geographical and solar/magnetic parameters. There is a smooth transition from mixing to diffusive equilibrium near 105 km. The density profiles for mixing conditions are calculated using the mean molecular weight for the lower atmosphere with the diffusive and mixing profiles equal at the turbopause. As with atomic oxygen and hydrogen an additional flow term was used with atomic nitrogen to produce a peak in the profile in the lower thermosphere. The shape of the atomic nitrogen profile was guided by the theoretical calculations of Gerard et al. [1984].

The basic expansion formula (equation (A22)) used to express the exospheric temperature and other parameters as a function of local time, latitude, longitude, UT, $F_{10.7}$, and Ap has been augmented over that used in MSIS-83 with terms to express hemispherical and seasonal differences in the polar regions and local time variations in the magnetic activity effect. Some time independent and longitude/UT terms were dropped for lack of significance.

In addition to the data from the OGO-6, San Marco-3, Aeros-A, AE-C,-D, -E, and ESRO-4 satellites, numerous rockets, and the Millstone Hill, St. Santin, Arecibo, Jicamarca, and Malvern incoherent scatter stations, all detailed by Hedin [1983], the model incorporates new incoherent scatter temperature data from St. Santin, composition data from the NACS instrument [Carignan et al., 1981] and temperature data from the WATS instrument [Spencer et al., 1981] of the DE-B satellite, and atomic nitrogen data from the AE-C,-D,-E [Mauersberger et al., 1975; Engebretson et al., 1977; Engebretson and Mauersberger, 1983], and DE-B satellites [Engebretson and Nelson, 1985]. In part because of calibration problems, the absolute density values (particularly N_2) from Dynamics Explorer were low relative to other satellites (see Table 2) and were not considered as reliable as for other satellites. For this reason, the data fitting was carried out with a fitting parameter times the DE (NACS) densities, and similarly for the AE-C (NATE) densities (also not reliably calibrated). Thus, while relative variations were fully influential in determining model parameters, the absolute values of the DE (NACS) and AE-C (NATE) densities had no influence on the overall average model density. The WATS temperature data were adjusted to account for the effect of typical high latitude winds along the satellite track found by the FPI instrument on DE-B [Hays et al., 1981] and for some internal instrument mode differences.

As discussed by Hedin [1983], temperatures determined from ground based optical techniques [e.g., Hernandez, 1982] often differ considerably from earlier MSIS models and also drag models. Little progress has been made in

Paper number 6A8712.

TABLE 1a. Model Coefficients

	T_∞	He	O	O_2	Ar	H	N
Average	1.037E+03	2.577E+13	8.002E+16	3.074E+16	1.155E+15	2.246E+11	5.736E+14
a10	0.000E+00	-5.045E-02	-1.052E-02	0.000E+00	0.000E+00	-4.166E-02	1.015E-01
a20	3.855E-02	-2.884E-02	-1.387E-01	1.380E-01	2.364E-01	-2.105E-01	-3.987E-01
a40	3.034E-03	-2.071E-01	-1.335E-01	0.000E+00	1.343E-01	-1.779E-01	0.000E+00
f00.a1	1.644E-03	-6.976E-04	4.777E-04	0.000E+00	0.000E+00	-5.959E-03	5.117E-03
f00.a2	-6.215E-06	2.065E-06	0.000E+00	0.000E+00	0.000E+00	3.845E-05	0.000E+00
F00.a1	3.117E-03	7.653E-04	2.744E-03	-1.518E-03	0.000E+00	-1.360E-02	9.951E-03
F00.a2	-6.411E-06	0.000E+00	0.000E+00	0.000E+00	0.000E+00	0.000E+00	0.000E+00
F10.c1	4.264E-03	-3.293E-03	0.000E+00	0.000E+00	0.000E+00	0.000E+00	0.000E+00
F11.a1	5.118E-03	1.678E-03	2.321E-03	0.000E+00	0.000E+00	-6.084E-03	1.184E-03
k00.a	5.333E-03	-6.299E-03	-5.811E-03	8.845E-03	1.570E-02	-1.984E-02	2.382E-03
k20.a	5.083E-03	-4.667E-02	-3.188E-02	1.452E-02	1.784E-02	-1.269E-02	-2.888E-02
k40.a	2.047E-03	-4.078E-03	-8.149E-03	0.000E+00	0.000E+00	1.325E-02	-1.882E-02
k10.c1	-8.377E-04	-3.727E-03	3.062E-03	0.000E+00	-6.020E-03	-4.950E-03	-7.653E-03
k30.c1	2.423E-03	-1.881E-02	-4.651E-03	0.000E+00	1.691E-02	-1.364E-02	-2.090E-04
k50.c1	4.738E-03	-1.018E-02	-9.734E-03	0.000E+00	0.000E+00	-1.150E-02	-1.574E-02
k11.a	6.724E-04	8.381E-03	2.429E-03	0.000E+00	1.293E-02	-5.869E-03	-8.607E-03
k31.a	1.089E-03	1.839E-03	-4.013E-03	0.000E+00	2.696E-03	-1.417E-03	-1.199E-02
k51.a	9.723E-04	-7.053E-04	-2.191E-03	0.000E+00	0.000E+00	2.137E-03	-6.464E-03
t11.k	4.682E+00	-4.066E+00	3.113E+00	0.000E+00	3.922E+00	2.638E+00	-3.001E+00
k00.s	1.131E-01	1.112E-01	9.882E-02	1.131E-01	1.131E-01	1.131E-01	1.131E-01
k00.r	1.691E-01	1.088E-01	9.405E-02	1.691E-01	1.691E-01	1.691E-01	1.691E-01
c00.1	8.055E-03	-8.410E-02	9.824E-02	5.966E-02	5.175E-02	4.965E-02	9.282E-02
t00.c1	3.001E+01	-1.508E+02	-8.733E+00	9.488E+00	3.427E+02	1.463E+02	5.677E+01
c00.2	1.424E-02	2.671E-01	1.186E-01	2.811E-02	-5.340E-02	1.540E-02	-1.767E-01
c20.2	0.000E+00	-5.960E-02	-2.045E-02	0.000E+00	0.000E+00	0.000E+00	6.504E-02
t00.c2	1.258E+02	1.050E+02	1.033E+02	7.360E+01	1.141E+02	7.342E+01	1.435E+00
c10.1	-1.274E-01	1.409E+00	3.721E-01	6.898E-02	-3.125E-01	4.361E-01	-2.116E-01
c30.1	-3.024E-02	1.750E-01	2.960E-02	0.000E+00	0.000E+00	1.076E-01	-1.599E-01
t10.c1	-8.454E+00	-7.429E+00	-7.789E+00	-8.454E+00	-2.236E+01	-9.581E+00	6.516E+00
c10.2	-1.926E-02	5.257E-02	5.173E-02	0.000E+00	0.000E+00	0.000E+00	4.762E-02
t10.c2	2.759E+00	-3.115E+01	-1.530E+01	0.000E+00	0.000E+00	0.000E+00	2.352E+01
a11	-1.055E-01	-1.033E-01	-5.295E-02	3.237E-04	1.031E-02	2.189E-01	-5.296E-01
a31	-6.071E-03	-7.024E-03	-4.450E-03	0.000E+00	0.000E+00	2.884E-02	-5.822E-03
a51	0.000E+00	-1.307E-02	0.000E+00	0.000E+00	0.000E+00	0.000E+00	0.000E+00
c21.1	1.235E-02	1.874E-02	1.205E-02	0.000E+00	4.374E-02	3.308E-02	-1.710E-04
b11	-1.156E-01	4.089E-01	5.981E-02	7.075E-02	-1.578E-01	2.910E-01	-6.793E-01
b31	2.022E-03	-9.199E-03	-3.629E-02	0.000E+00	0.000E+00	2.174E-02	-1.677E-01
b51	0.000E+00	-2.243E-02	0.000E+00	0.000E+00	0.000E+00	0.000E+00	0.000E+00
d21.1	-5.263E-03	1.110E-01	5.220E-02	0.000E+00	-3.541E-02	4.006E-02	-1.159E-01
a22	-5.163E-04	1.297E-02	1.353E-02	-9.109E-03	-3.792E-03	1.901E-02	7.142E-02
a42	-1.174E-03	0.000E+00	5.577E-03	0.000E+00	0.000E+00	0.000E+00	1.518E-02
c32.1	3.866E-03	0.000E+00	0.000E+00	0.000E+00	0.000E+00	0.000E+00	0.000E+00
b22	9.902E-03	-1.887E-02	-3.128E-02	-5.167E-02	-5.876E-02	-1.052E-02	-6.424E-02
b42	-3.546E-04	0.000E+00	-4.542E-04	0.000E+00	0.000E+00	0.000E+00	-1.927E-02
d32.1	3.891E-03	0.000E+00	0.000E+00	0.000E+00	0.000E+00	0.000E+00	0.000E+00

Read for example f00.a1 as f_{00}^{a1}

resolving these differences and inclusion of these data would obscure rather than clarify the differences before they are better understood. Similar optical measurements were made from the DE-B satellite [Hays et al., 1981] and complete processing and comparisons with temperatures from the WATS instrument have not been completed. It is hoped that future comparisons of the satellite optical data, models, and other data will lead to a better understanding of the accuracy of each.

The final model coefficients are given in Table 1. For the most part only coefficients/terms are given in which the statistical error from the fit is estimated to be less than a third of the coefficient value. An exception was made for flow correction coefficients (equations (A20) and (A21)) which are sometimes poorly determined given a lack of constraining data. A tabulation of coefficient error and correlation coefficients is available from the author. The annual phases for O_2, N_2, and lower thermosphere temperature parameters were set to agree with those of exospheric temperature.

The average departures and standard deviations of the individual data subsets used in generating the model are given in Table 2, and these can be used as rough indicators of how

TABLE 1b. Model Coefficients

	T_∞	He	O	O_2	Ar	H	N
a33	3.413E-04	2.758E-03	9.618E-04	0.000E+00	-1.162E-03	-1.476E-03	5.762E-03
c43.1	-1.532E-04	0.000E+00	0.000E+00	0.000E+00	0.000E+00	0.000E+00	0.000E+00
c63.1	1.151E-04	0.000E+00	0.000E+00	0.000E+00	0.000E+00	0.000E+00	0.000E+00
b33	1.473E-03	-3.134E-03	-3.489E-03	0.000E+00	-3.663E-03	-1.047E-04	4.759E-03
d43.1	-1.739E-04	0.000E+00	0.000E+00	0.000E+00	0.000E+00	0.000E+00	0.000E+00
d63.1	3.650E-05	0.000E+00	0.000E+00	0.000E+00	0.000E+00	0.000E+00	0.000E+00
a21.0	5.626E-03	-1.799E-02	-1.054E-02	-1.489E-02	-1.207E-02	-9.203E-03	7.978E-04
a41.0	5.941E-03	-1.583E-02	-9.457E-03	-7.872E-03	1.367E-02	-2.091E-02	-7.705E-03
a61.0	1.094E-03	-7.123E-03	-1.598E-03	0.000E+00	1.360E-02	-1.341E-02	1.910E-03
a11.0	-3.018E-03	8.046E-03	1.283E-02	0.000E+00	0.000E+00	0.000E+00	0.000E+00
a31.0	-4.236E-03	1.011E-02	7.886E-03	0.000E+00	0.000E+00	0.000E+00	0.000E+00
a51.0	-2.483E-03	8.733E-03	7.972E-03	0.000E+00	0.000E+00	0.000E+00	0.000E+00
a11.c1	1.897E-03	3.964E-02	-2.985E-02	0.000E+00	2.906E-02	0.000E+00	0.000E+00
a31.c1	4.157E-03	-2.138E-02	-1.266E-02	0.000E+00	3.490E-03	0.000E+00	0.000E+00
b21.0	-1.165E-02	4.076E-02	4.343E-02	-6.834E-02	-2.651E-02	5.980E-02	1.590E-02
b41.0	-4.492E-03	2.823E-02	1.140E-02	-4.418E-02	-2.091E-02	6.333E-03	-1.914E-03
b61.0	-3.532E-04	9.081E-03	-6.184E-03	0.000E+00	-1.095E-02	-1.129E-03	-3.428E-02
b11.0	9.193E-04	2.383E-02	-1.208E-02	0.000E+00	0.000E+00	0.000E+00	0.000E+00
b31.0	2.164E-03	4.804E-03	-7.675E-03	0.000E+00	0.000E+00	0.000E+00	0.000E+00
b51.0	8.640E-04	1.711E-03	-1.208E-03	0.000E+00	0.000E+00	0.000E+00	0.000E+00
b11.c1	1.181E-02	-1.026E-01	-5.683E-02	0.000E+00	5.012E-02	0.000E+00	0.000E+00
b31.c1	3.312E-03	-5.917E-03	-1.530E-02	0.000E+00	5.506E-02	0.000E+00	0.000E+00
F21.a0	2.922E-03	-6.335E-03	-3.290E-03	0.000E+00	0.000E+00	0.000E+00	0.000E+00
a10.1	-1.334E-02	2.535E-02	-1.685E-02	0.000E+00	0.000E+00	-4.833E-02	1.010E-02
a30.1	-2.434E-02	8.530E-02	-1.130E-01	0.000E+00	0.000E+00	8.309E-02	1.165E-01
a50.1	-1.357E-02	1.022E-01	-6.366E-02	0.000E+00	0.000E+00	9.880E-02	-3.122E-03
t10.a1	3.114E+04	2.950E+04	-1.377E+04	0.000E+00	0.000E+00	-1.411E+04	1.398E+04
r10.a1	-5.654E-01	-4.052E-01	-3.026E-01	0.000E+00	0.000E+00	0.000E+00	0.000E+00
r10.c1	0.000E+00	6.035E-01	0.000E+00	0.000E+00	0.000E+00	0.000E+00	0.000E+00
a32.1	8.456E-04	-6.191E-03	-5.861E-03	0.000E+00	8.355E-03	0.000E+00	0.000E+00
a52.1	5.387E-04	-2.693E-03	-2.531E-03	0.000E+00	4.194E-03	0.000E+00	0.000E+00
t32.a1	2.480E+02	-5.202E+02	-2.548E+03	0.000E+00	1.204E+04	0.000E+00	0.000E+00
k21.a0	1.373E-03	-6.428E-03	1.600E-03	0.000E+00	1.278E-02	-1.257E-03	7.601E-03
k41.a0	9.958E-04	-1.717E-03	-3.882E-03	0.000E+00	-2.080E-03	1.528E-03	2.594E-03
k61.a0	0.000E+00	0.000E+00	-1.648E-03	0.000E+00	-4.618E-03	1.305E-03	1.723E-03
λ21.k0	-1.090E+02	-6.791E+01	-7.480E+01	0.000E+00	-6.294E+01	7.556E+00	7.792E+01
r21.k0	0.000E+00	-6.176E-01	0.000E+00	0.000E+00	0.000E+00	0.000E+00	0.000E+00
k10.a1	7.477E-05	-6.024E-03	-2.764E-03	0.000E+00	-1.000E-02	6.734E-03	-3.205E-03
k30.a1	8.880E-04	-4.071E-03	9.679E-03	0.000E+00	-2.333E-03	2.017E-03	-2.070E-02
k50.a1	0.000E+00	5.423E-03	0.000E+00	0.000E+00	9.724E-03	0.000E+00	0.000E+00
t10.k1	-2.830E+03	-6.846E+03	-1.524E+04	0.000E+00	1.925E+04	-1.055E+03	-1.307E+03
k11.c1	1.202E-03	2.709E-03	0.000E+00	0.000E+00	-9.559E-03	0.000E+00	0.000E+00
λ11.kc	-3.072E+00	-1.750E+02	0.000E+00	0.000E+00	-1.517E+03	0.000E+00	0.000E+00

consistently a particular quantity can be measured and how well it can be represented by the model. For the most part the data set differences are not beyond reasonable bounds for the current state of the art in absolute thermospheric measurements. The largest scatter between and within data sets occurs for the minor constituents helium, atomic nitrogen, and argon.

It must be remembered that global coverage for density and temperature, and particularly composition, is very sparse between 90 and 150 km and so the model predictions for this altitude range are not expected to be as representative of the real atmosphere as at higher altitudes. Because of sparse coverage several of the variations detected in the upper thermosphere could not be reliably determined in the lower thermosphere. Similarly, data again become very sparse in the exosphere above 600 km and upward extrapolations are expected to become increasingly inaccurate at higher altitudes.

3. Model Predictions and Comparisons

3.1. Mean, Time-Independent, and Solar Activity

The global and time averaged temperature profiles for MSIS-86 are within 1% of the MSIS-83 temperatures and the densities within 10%. The average exospheric temperature and total density at various solar activity levels are shown in Figure 1 and are nearly identical with MSIS-83 and within 10% of J77 [Jacchia, 1977]. The exospheric temperature and number density of all constituents except hydrogen and molecular oxygen increase with solar activity (solar EUV radiation).

TABLE 1c. Model Coefficients

	T_∞	He	O	O_2	Ar	H	N
Coefficients for alternate formulation with three hour indices							
k00.a	6.091E-03	-9.167E-03	-6.002E-03	1.079E-02	1.629E-02	-2.576E-02	-3.689E-03
k20.a	7.773E-03	-5.979E-02	-3.277E-02	2.297E-02	2.173E-02	-1.286E-02	-3.454E-02
k40.a	2.308E-03	-2.047E-03	-3.786E-03	0.000E+00	0.000E+00	1.566E-02	-1.926E-02
k10.c1	-3.150E-04	-5.093E-03	3.233E-03	0.000E+00	-8.477E-03	-8.342E-03	-9.325E-03
k30.c1	4.001E-03	-2.843E-02	-6.395E-03	0.000E+00	1.169E-02	-1.873E-02	-1.502E-02
k50.c1	5.150E-03	-1.242E-02	-6.631E-03	0.000E+00	0.000E+00	-1.909E-02	-8.678E-03
k11.a	1.630E-03	1.337E-02	-3.044E-04	0.000E+00	1.490E-02	-8.038E-03	-7.648E-03
k31.a	1.088E-03	3.934E-03	-4.019E-03	0.000E+00	5.445E-03	-2.843E-03	-1.315E-02
k51.a	9.953E-04	-5.037E-04	-1.187E-03	0.000E+00	0.000E+00	2.567E-03	-6.767E-03
t11.k1	4.190E+00	-4.577E+00	4.152E+00	0.000E+00	5.649E+00	1.714E+00	-1.824E+00
k00.s	1.324E-01	1.268E-01	7.578E-02	1.324E-01	1.324E-01	1.324E-01	1.324E-01
k00.r	2.133E-01	1.289E-01	1.714E-01	2.133E-01	2.133E-01	2.133E-01	2.133E-01
β00	4.050E-05	3.450E-05	2.777E-05	2.999E-05	3.170E-05	3.190E-05	3.147E-05
β10	5.802E-03	3.232E-03	0.000E+00	0.000E+00	0.000E+00	0.000E+00	0.000E+00
k21.a0	1.530E-03	-9.718E-03	-3.220E-03	0.000E+00	1.280E-02	0.000E+00	8.822E-03
k41.a0	6.452E-04	-2.066E-03	-2.283E-03	0.000E+00	-1.894E-03	0.000E+00	1.716E-03
k61.a0	0.000E+00	0.000E+00	-7.067E-04	0.000E+00	-5.372E-03	0.000E+00	2.727E-03
λ21.k0	-9.118E+01	-7.318E+01	-6.716E+01	0.000E+00	-7.124E+01	0.000E+00	8.945E+01
r21.k0	-3.641E-01	-5.295E-01	-2.019E-01	0.000E+00	0.000E+00	0.000E+00	0.000E+00
k10.a1	1.553E-03	-7.869E-03	-3.348E-03	0.000E+00	-7.046E-03	1.036E-02	-2.587E-03
k30.a1	1.337E-03	-7.983E-03	-1.707E-03	0.000E+00	2.079E-03	1.058E-03	-2.199E-02
k50.a1	-1.823E-03	5.365E-03	0.000E+00	0.000E+00	6.367E-03	0.000E+00	0.000E+00
t10.k1	-2.630E+02	-5.312E+03	6.362E+03	0.000E+00	2.299E+04	3.579E+03	4.387E+03
k11.c1	1.702E-03	-4.258E-03	0.000E+00	0.000E+00	-7.722E-03	0.000E+00	0.000E+00
λ11.kc	-3.201E+00	1.915E+01	0.000E+00	0.000E+00	-7.340E+01	0.000E+00	0.000E+00

The temperature at 120 km increases with $F_{10.7}$, in agreement with incoherent scatter [Wand, 1983a], as does the mesopause height. The temperature gradient at 120 km also increases with solar activity, although the shape factor s in the Bates temperature profile decreases with solar activity in agreement with incoherent scatter [Oliver, 1979].

Over much of the thermosphere the temperature, and the N_2, O_2, and Ar, densities increase toward the poles under magnetically quiet conditions, while the densities of O, N, He, and H decrease.

As shown in Figure 2, atomic nitrogen, guided by theory, has a peak near 200 km. There is not, however, a rapid drop near the winter pole as calculated by Gerard et al. [1984].

3.2. Yearly Variations

Contours of diurnally averaged temperature and density as a function of latitude and day of year for 400 km are shown in Figure 3. The temperature and species heavier than atomic oxygen have predominantly asymmetrical annual (seasonal) variations with summer maxima while the lighter species, except atomic nitrogen, have winter maxima. Atomic oxygen has a winter maximum at lower altitudes and a summer maximum at higher altitudes. The winter helium bulge varies with solar activity. It is roughly a factor of 10, 20, and 40 for 10.7 levels of 70, 150, and 230, respectively.

While the symmetrical semiannual variation, maximizing near the equinoxes, is most prominent for atomic oxygen and molecular nitrogen, all

TABLE 1d. Model Coefficients

	T_∞	He	O	O_2	Ar	H	N
Ω		6.711E-06	1.294E-01	2.683E-01	1.196E-02	2.538E-06	1.533E-01
z_h		1.000E+02	1.050E+02	1.050E+02	1.050E+02	9.500E+01	1.050E+02
z_1		1.275E+02	1.204E+02	1.144E+02	1.216E+02	1.219E+02	1.027E+02
H_1		4.711E+00	5.250E+01	7.671E+00	1.756E+01	2.334E+01	5.474E+01
z_2			7.169E+01			7.586E+01	8.274E+01
H_2			8.630E+00			2.084E+00	3.282E+01
R_2			-3.258E+01			-1.602E+01	-3.417E+01

TABLE 1e. Model Coefficients

	N_2	T_ℓ	z_o	T_o	T_R	T_ℓ'
Average	3.004E+17	3.770E+02	9.442E+01	1.803E+02	1.528E-01	1.586E+01
a20	0.000E+00	0.000E+00	-2.438E-02	-7.680E-02	1.163E+00	-4.675E-02
a40						1.203E-01
F00.a1	3.771E-04	5.685E-04	1.900E-04	0.000E+00	0.000E+00	2.523E-03
k00.a	0.000E+00	4.668E-03	0.000E+00	0.000E+00	0.000E+00	0.000E+00
k20.a	0.000E+00	6.642E-03	0.000E+00	0.000E+00	0.000E+00	0.000E+00
k00.s	1.131E-01	1.131E-01	1.131E-01	1.131E-01	1.131E-01	1.131E-01
k00.r	1.691E-01	1.691E-01	1.691E-01	1.691E-01	1.691E-01	1.691E-01
c00.1	8.985E-02	0.000E+00	0.000E+00	0.000E+00	0.000E+00	0.000E+00
t00.c1	-2.363E+01	0.000E+00	0.000E+00	0.000E+00	0.000E+00	0.000E+00
c00.2	2.082E-02	1.077E-02	0.000E+00	-1.380E-02	0.000E+00	0.000E+00
t00.c2	1.396E+02	8.938E+01	0.000E+00	-1.401E+00	0.000E+00	0.000E+00
c10.1	-1.194E-01	-1.924E-02	5.221E-02	1.205E-01	-6.492E-01	-1.332E-01
c30.1	0.000E+00	0.000E+00	0.000E+00	7.445E-02	0.000E+00	0.000E+00
t10.c1	-8.454E+00	-8.454E+00	-8.454E+00	-8.454E+00	-8.454E+00	-8.454E+00
a11	3.662E-03	-2.002E-02	0.000E+00	0.000E+00	0.000E+00	0.000E+00
b11	-1.789E-03	-1.958E-03	0.000E+00	0.000E+00	0.000E+00	0.000E+00
a22	1.904E-02	-9.384E-03	7.673E-03	9.877E-03	-5.849E-02	1.914E-02
a42	6.323E-03	-2.601E-03	-2.706E-03	-6.888E-04	2.992E-02	7.877E-03
c32.1						-9.734E-03
c52.1	0.000E+00	5.117E-05	1.371E-03	0.000E+00	0.000E+00	0.000E+00
b22	-3.923E-02	1.315E-02	5.645E-03	1.753E-03	-1.021E-01	1.254E-03
b42	5.481E-03	-8.086E-04	-5.265E-04	2.870E-03	-4.862E-02	-2.337E-03
d32.1						-7.185E-04
d52.1	0.000E+00	2.557E-03	1.331E-03	0.000E+00	0.000E+00	0.000E+00
a33	-3.998E-06	0.000E+00	0.000E+00	0.000E+00	0.000E+00	0.000E+00
b33	-2.430E-03	0.000E+00	0.000E+00	0.000E+00	0.000E+00	0.000E+00
Coefficients for alternate formulation with three hour indices						
k00.a	0.000E+00	5.820E-03	0.000E+00	0.000E+00	0.000E+00	0.000E+00
k20.a	0.000E+00	6.220E-03	0.000E+00	0.000E+00	0.000E+00	0.000E+00
k00.s	1.324E-01	1.324E-01	1.324E-01	1.324E-01	1.324E-01	1.324E-01
k00.r	2.133E-01	2.133E-01	2.133E-01	2.133E-01	2.133E-01	2.133E-01
ß00	0.000E+00	2.415E-05	0.000E+00	0.000E+00	0.000E+00	0.000E+00

species have a significant semiannual variation. There is a 5 to 10% symmetrical annual variation, maximizing near the end of the year for all species except hydrogen, which when combined with the semiannual variation leads to a principal minimum in July and principal maximum in October at equatorial latitudes. The temperature and N_2 semiannual variations are somewhat stronger in the northern hemisphere, while the oxygen, helium, and atomic nitrogen semiannual variations are stronger in the southern hemisphere.

At higher latitudes the symmetrical annual component when combined with the seasonal (asymmetrical annual) component leads to larger annual variations in He and (at lower altitudes) O densities for the northern hemisphere.

The annual variations of atomic nitrogen are very similar to those deduced by Kohnlein et al. [1979] from AEROS satellite data.

3.3. Daily Variations

Contours of annually averaged temperature and density as a function of local time and latitude at 400 km are shown in Figure 4. At 400 km the variations are predominantly diurnal (24-hour period), with temperature and the heavier species maximizing near 16 hours local time. Atomic oxygen maximizes near 14 hours local time, while helium and hydrogen maximize near 7 and 3 hours local time. The phase and amplitude of the diurnal, semidiurnal, and terdiurnal temperature variations depend on season so that the temperature maximum is broader in summer than in winter. Below 160 km the semidiurnal variation becomes predominant in density [Sharp et al., 1978] and in temperature, with peak semidiurnal temperature amplitudes occurring between 100 and 120 km [Wand, 1983b].

3.4. Magnetic Activity Variations

Contours of diurnally averaged temperature and natural logarithm of density departures from quiet conditions for an Ap of 100 as a function of day and latitude at 120 and 400 km are shown in Figure 5 for June solstice conditions. Near the equator the temperature and densities of all species except hydrogen increase somewhat with

TABLE 2a. Density Ratio to MSIS 1986 for N_2, O, and He when Ap<11

Data Set	altitude	N_2 avg	N_2 sd	N_2 pts	O avg	O sd	O pts	He avg	He sd	He pts
OGO-6 (MS)	400-700	1.08	0.26	597	1.17	0.15	1146	1.18	0.18	1114
San Marco-3 (MS)	190-250	1.08	0.21	65	0.93	0.16	41	1.10	0.15	46
Aeros-A NATE (MS)	200-500	1.12	0.43	316	1.16	0.30	611	1.16	0.36	546
AE-C NATE (MS)	190-400	1.04	0.29	555	0.89	0.18	1114	0.69	0.15	980
AE-C OSS (MS)	135-160+	0.97	0.15	496						
AE-C OSS (MS)	190-400	0.97	0.22	293	1.06	0.17	542	1.04	0.21	479
AE-D OSS (MS)	140-160+	0.96	0.16	210						
AE-D OSS (MS)	190-400	0.88	0.22	73	0.99	0.18	126	0.79	0.21	129
AE-E NACE (MS)	140-160+	1.01	0.12	941						
AE-E NACE (MS)	190-450	1.00	0.22	619	0.89	0.19	1362	0.93	0.14	1224
ESRO-4 (MS)	200-350	0.87	0.32	370	0.83	0.24	746	0.86	0.32	606
DE-B NACS (MS)	200-900	0.60	0.22	743	0.89	0.15	2037	0.86	0.16	2106
Rockets (MS)	100-120	0.83	0.36	35						
Rockets (MS)	110-160	0.96	0.29	122						
Rockets (MS)	190-300	0.89	0.26	94						
Arecibo (IS)	100-120	0.92	0.32	228						
Arecibo (IS)	110-135	1.16	0.52	132						

avg is average
sd is standard deviation
pts is points

increasing magnetic activity. Much larger changes occur near the poles with temperature and neutral species heavier than atomic nitrogen increasing with higher magnetic activity and lighter species decreasing. At lower altitudes atomic oxygen density near the poles decreases with increasing activity, while at higher altitudes atomic oxygen density increases.

There are also seasonal differences seen in Figure 5. Unlike MSIS-83, the greatest

TABLE 2b. Density Ratio to MSIS 1986 for Ar, O_2, and H when Ap<11

Data Set	altitude	Ar avg	Ar sd	Ar pts	O_2 avg	O_2 sd	O_2 pts	H avg	H sd	H pts
San Marco-3 (MS)	190-250	1.11	0.36	83						
Aeros-A NATE (MS)	200-350	1.36	0.54	452						
AE-C NATE (MS)	250-350	1.30	0.36	337						
AE-C OSS (MS)	140-250	0.93	0.32	262	0.93	0.27	218			
AE-C EUVS (absorp)	100				0.99	0.27	121			
AE-C EUVS (absorp)	130				1.25	0.21	54			
AE-C EUVS (absorp)	150				1.07	0.32	130			
AE-D OSS (MS)	140-250	1.41	0.54	143	1.17	0.35	511			
AE-E NACE (MS)	140-300	1.04	0.21	644						
AE-E OSS (MS)	140-250				1.20	0.21	297			
AE-E EUVS (absorp)	100				0.99	0.31	249			
AE-E EUVS (absorp)	130				0.96	0.19	175			
AE-E EUVS (absorp)	150				0.80	0.16	296			
ESRO-4 (MS)	200-300	0.83	0.40	1035						
DE-B NACS (MS)	200-400	0.83	0.41	1038						
Rockets (MS)	140-200	0.93	0.36	65						
Rockets (MS)	130-220				0.94	0.32	281			
Rockets (absorp)	120-150				0.88	0.30	14			
AE-C BIMS (IMS)	200-500							1.01	0.26	2124
AE-C MIMS (IMS)	160-300							1.27	0.03	8
AE-E BIMS (IMS)	200-500							0.98	0.26	1596

absorp is absorption
MS is mass spectrometer
IMS is ion mass spectrometer

TABLE 2c. Temperature Difference and Total Density Ratio to MSIS 1986 when Ap>11

Data Set	altitude	Temperature avg	Temperature sd	Temperature pts	Density avg	Density sd	Density pts
Millstone Hill (IS)	100-120	1.	45.	883			
Millstone Hill (IS)	110-130	3.	42.	934			
Millstone Hill (IS)	exospheric	22.	46.	256			
St. Santin (IS)	exospheric	-9.	47.	276			
Arecibo (IS)	100-120	-3.	26.	697			
Arecibo (IS)	110-135	-1.	29.	876			
Arecibo (IS)	250-exospheric	22.	36.	158			
Jicamarca (IS)	exospheric	-36.	49.	31			
Malvern (IS)	240-400	-31.	65.	78			
AE-C NATE (MS)	135-160	-13.	64.	249			
AE-C NATE (MS)	190-300	-42.	107.	223			
AE-D NATE (MS)	140-160	10.	48.	107			
AE-D NATE (MS)	190-400	-12.	84.	213			
AE-E NATE (MS)	140-170	-11.	43.	461			
AE-E NATE (MS)	190-400	-29.	42.	427			
DE-B WATS (MS)	200-500	4.	72.	1136			
Rockets (MS)	100-120	-5.	29.	20			
Rockets (MS)	110-160	4.	44.	112			
Rockets (MS)	190-300	-31.	69.	91			
Rockets (gauge)	85-120	11.	24.	160	1.23	0.26	247
Rockets (gauge)	110-120	-22.	39.	17	1.25	0.20	59
Rockets (grenade)	85-110	0.	17.	309	0.99	0.18	310
Rockets (falling sphere)	85-120	1.	18.	140	1.13	0.28	201
Rockets (falling sphere)	110-120	-11.	33.	3	1.14	0.33	26

variations with magnetic activity occur near the winter pole, although the magnetic activity effects extend further toward the equator in summer so that at mid-latitudes the largest effects are found in summer consistent with incoherent scatter [Oliver, 1980]. Another new feature of the 1986 model is the maximum in magnetic activity effects in the midnight to early morning local time sector. The morphology of the magnetic activity effects for atomic nitrogen appear to be particularly complex with a decrease more likely in winter than summer and in the early evening rather than morning local time [Hedin and Engebretson, 1986].

As in MSIS-83 there is an alternate representation of storm effects using the 3-hour Ap index to provide a more realistic description of the time history of an event. The time constants found for the decay in storm response after an impulse event range from 7 to 12 hours on average. However, a latitude variation of the storm response time was allowed for in the 1986 model and for He and exospheric temperature that resulted in a significant pole to equator increase in time constant of 2 and 4 hours, respectively.

TABLE 2d. Density Ratio to MSIS 1986 for N when Ap<11

Data Set	altitude	avg	sd	pts
AE-C OSS (MS)	350-550	1.14	0.31	1916
AE-D OSS (MS)	275-475	0.74	0.32	2428
AE-E NACE (MS)	250-400	1.14	0.27	3202
DE-B NACS (MS)	200-500	0.33	0.66	196

3.5. Longitude/UT Variations

The effect of the longitude terms is to enhance temperature and density for the heaviest species in the general vicinity of the magnetic poles. In MSIS-86 these enhancements are more closely confined to the polar regions in winter than summer as suggested by the Dynamics Explorer data [Hedin and Carignan, 1985]. As with other variations, the lighter species tend to be depleted, particularly at lower altitudes, although atomic nitrogen is enhanced near the magnetic poles. Magnetic activity variations are also increased near the poles.

There is a 24-hour universal time (UT) variation of temperature and density in the polar regions [Hedin et al., 1979] with temperature peaking near 8.5 hours UT in the southern hemisphere and 20.5 hours in the northern. Amplitudes are larger in the southern hemisphere and increase with magnetic activity. This variation adds a 24 hour variation to the magnetic polar enhancements (depletions for lighter species), and combined with the longitude variations results in enhancements (or depletions) in the early morning magnetic local time.

Appendix: Model Formulation

The temperature profile

$$T(z) = T_\infty - (T_\infty - T_\ell) \exp\left[-\sigma\, \xi\, (z, z_\ell)\right]$$

$$z \geq z_a \qquad \text{(A1a)}$$

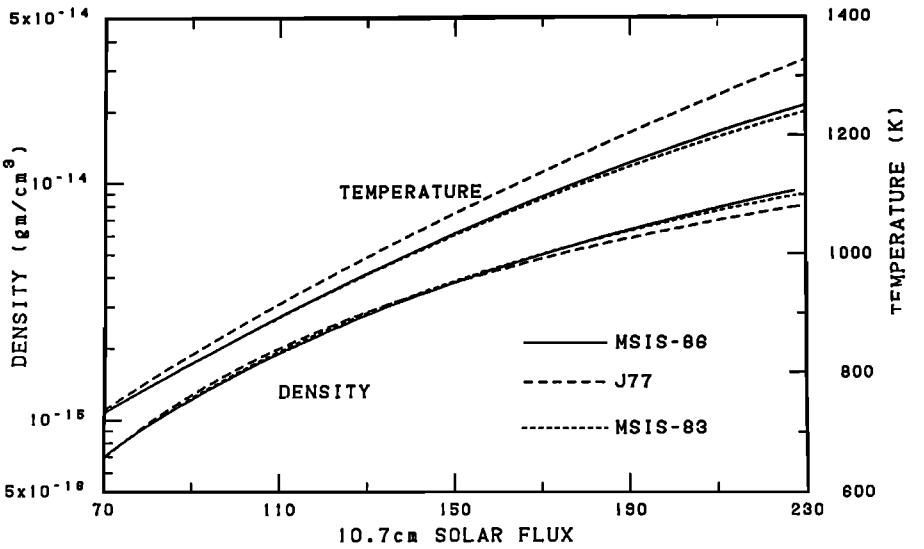

Fig. 1. Average MSIS-86 total mass density and temperature at 400 km vs $F_{10.7}$ with the J77 and MSIS-83 models shown for comparison.

$$T(z) = 1/(1/T_o + T_B\, x^2 + T_C\, x^4 + T_D\, x^6) \qquad z < z_a \qquad \text{(A1b)}$$

and matching temperature and temperature gradient at z_a,

$$T_a = T(z_a) = T_\infty - (T_\infty - T_\ell) \cdot \exp[-\sigma\, \xi\, (z_a, z_\ell)] \qquad \text{(A2a)}$$

$$T_a' = T'(z_a) = (T_\infty - T_a)\, \sigma\, [(R_p + z_\ell)/(R_p + z_a)]^2 \qquad \text{(A2b)}$$

gives

$$T_D = 0.66666\, \xi\, (z_o, z_a)\, T_a'/T_a^2 - 3.11111\, (1/T_a - 1/T_o) + 7.11111\, (1/T_{12} - 1/T_o) \qquad \text{(A3a)}$$

$$T_C = \xi\, (z_o, z_a)\, T_a'/(2\, T_a^2) - (1/T_a - 1/T_o) - 2\, T_D \qquad \text{(A3b)}$$

$$T_B = (1/T_a - 1/T_o) - T_C - T_D \qquad \text{(A3c)}$$

$$x = -[\xi\, (z, z_a) - \xi\, (z_o, z_a)]/\xi\, (z_o, z_a) \qquad \text{(A3d)}$$

$$T_{12} = T_o + T_R\, (T_a - T_o) \qquad \text{(A3e)}$$

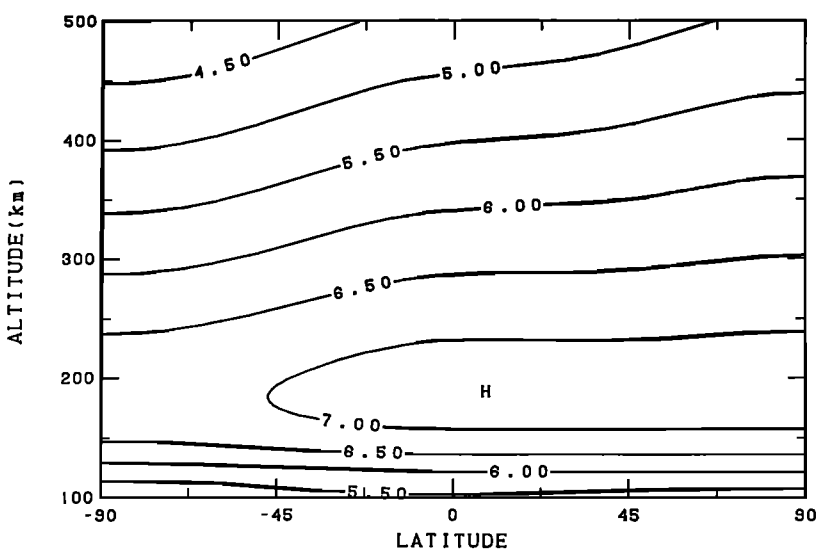

Fig. 2. Contour plot in altitude and latitude coordinates of diurnally averaged logarithm (base 10) MSIS-86 atomic nitrogen densities (cm^{-3}) for an $F_{10.7}$ of 80, Ap of 4, and summer solstice conditions.

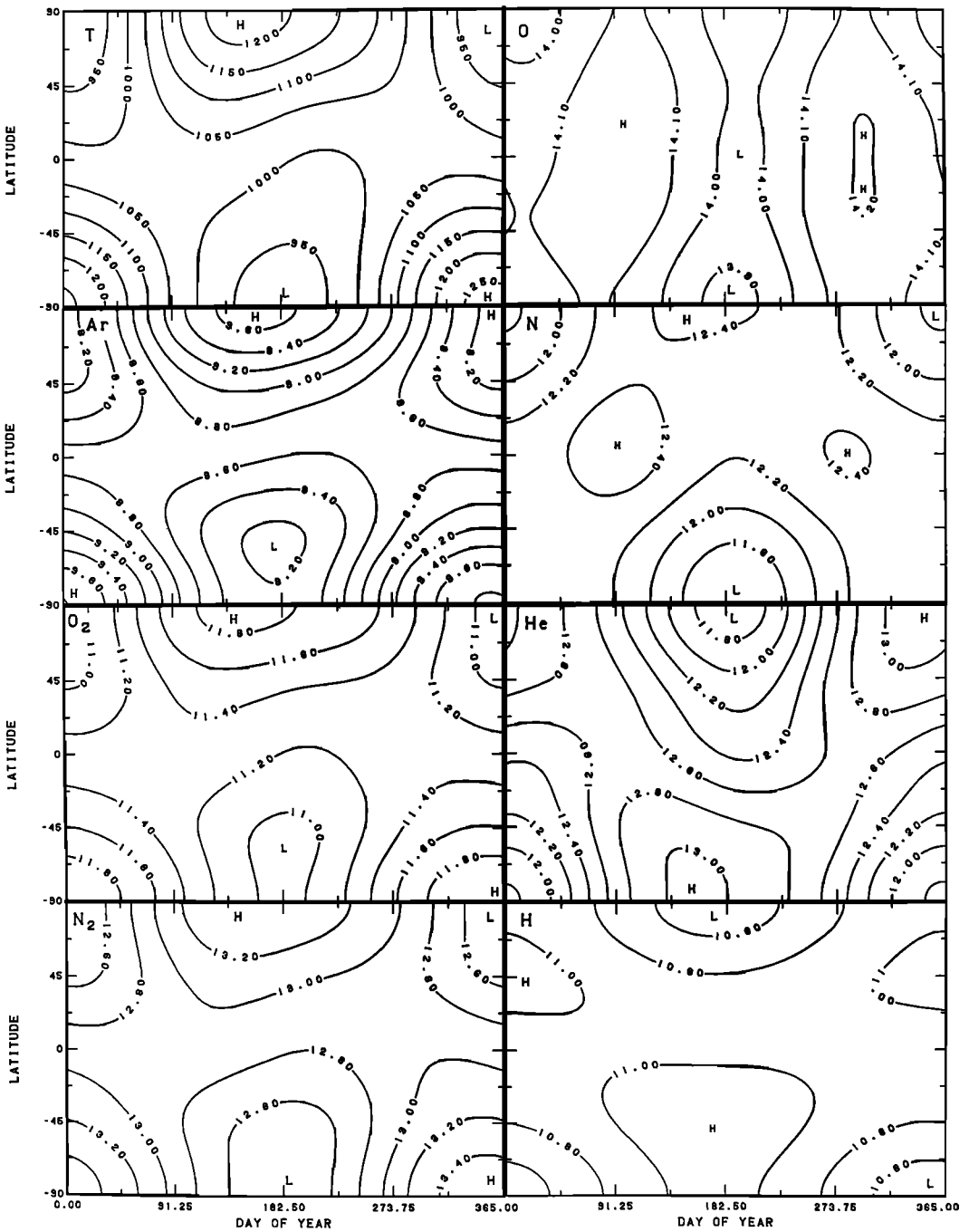

Fig. 3. Contour plot in latitude and day of year coordinates of diurnally averaged MSIS-86 model temperature and logarithm (base 10) Ar, O_2, N_2, O, N, He, and H densities (m^{-3}) at 400 km for an $F_{10.7}$ of 150 and Ap of 4.

$$\xi(z, z_\ell) = (z - z_\ell)\,(R_p + z_\ell)/(R_p + z) \quad \text{(A4a)}$$

$$\xi(z, z_a) = (z - z_a)\,(R_p + z_a)/(R_p + z) \quad \text{(A4b)}$$

$$\sigma = T_\ell'/(T_\infty - T_\ell) \quad \text{(A5)}$$

$$T_\ell' = \bar{T}_\ell'\,(1 + G(L)) \quad \text{(A6)}$$

$$T_\infty = \bar{T}_\infty\,[1 + G(L)] \quad \text{(A7)}$$

$$T_\ell = \bar{T}_\ell\,[1 + G(L)] \quad \text{(A8)}$$

$$T_o = \bar{T}_o\,[1 + G(L)] \quad \text{(A9)}$$

$$z_o = \bar{z}_o\,[1 + G(L)] \quad \text{(A10)}$$

$$T_R = \bar{T}_R\,[1 + G(L)] \quad \text{(A11)}$$

where

T ambient temperature, ^oK;
T_a, temperature at z_a, ^oK;
T_a' temperature gradient at z_a, $^oK/km$;

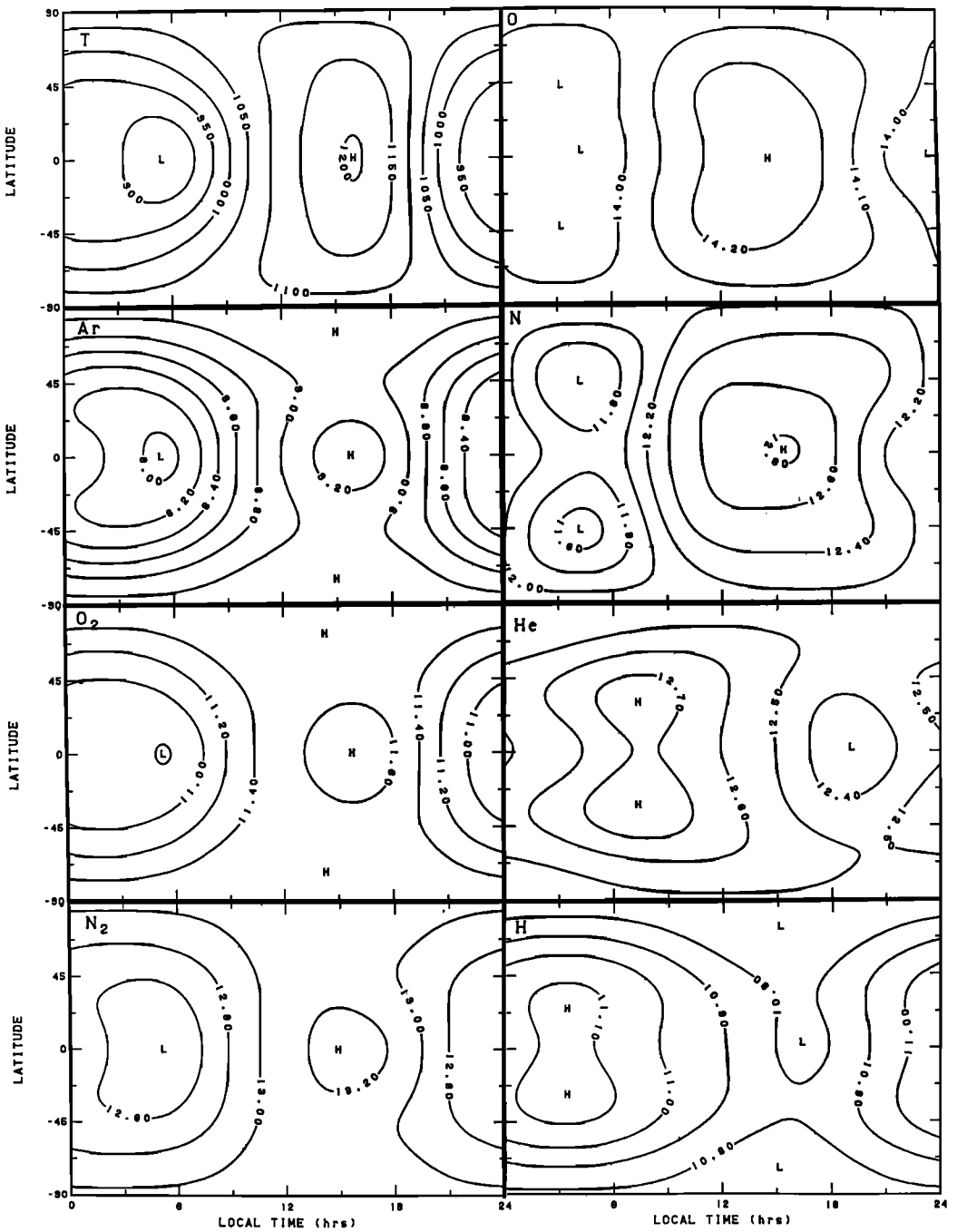

Fig. 4. Contour plot in latitude and local time coordinates of annually averaged MSIS-86 model temperature and logarithm (base 10) Ar, O_2, N_2, O, N, He, and H densities (m^{-3}) at 400 km for an $F_{10.7}$ of 150 and Ap of 4.

$\overline{T}_{12}$ temperature at $(z_o + z_\ell)/2$, °K;
$\overline{T}_\infty$ average exospheric temperature (fitting parameter), °K;
$\overline{T}_\ell$ average temperature at z_ℓ (fitting parameter), °K;
$\overline{T}_o$ average mesopause temperature (fitting parameter), °K;
$\overline{T}_\ell'$ average temperature gradient at z_ℓ (fitting parameter), °K/km;
$\overline{T}_R$ average mesopause shape parameter (fitting parameter);
z altitude, km;
z_ℓ 120 km;
z_a altitude of temperature profile junction (fitting parameter), 117.2 km;
$\overline{z}_o$ average mesopause height (fitting parameter), km;
R_p 6356.77 km.

The density profile is a meld of diffusive and mixing profiles multiplied by one or more factors $C_1 \ldots C_n$ to account for chemistry or dynamics flow effects

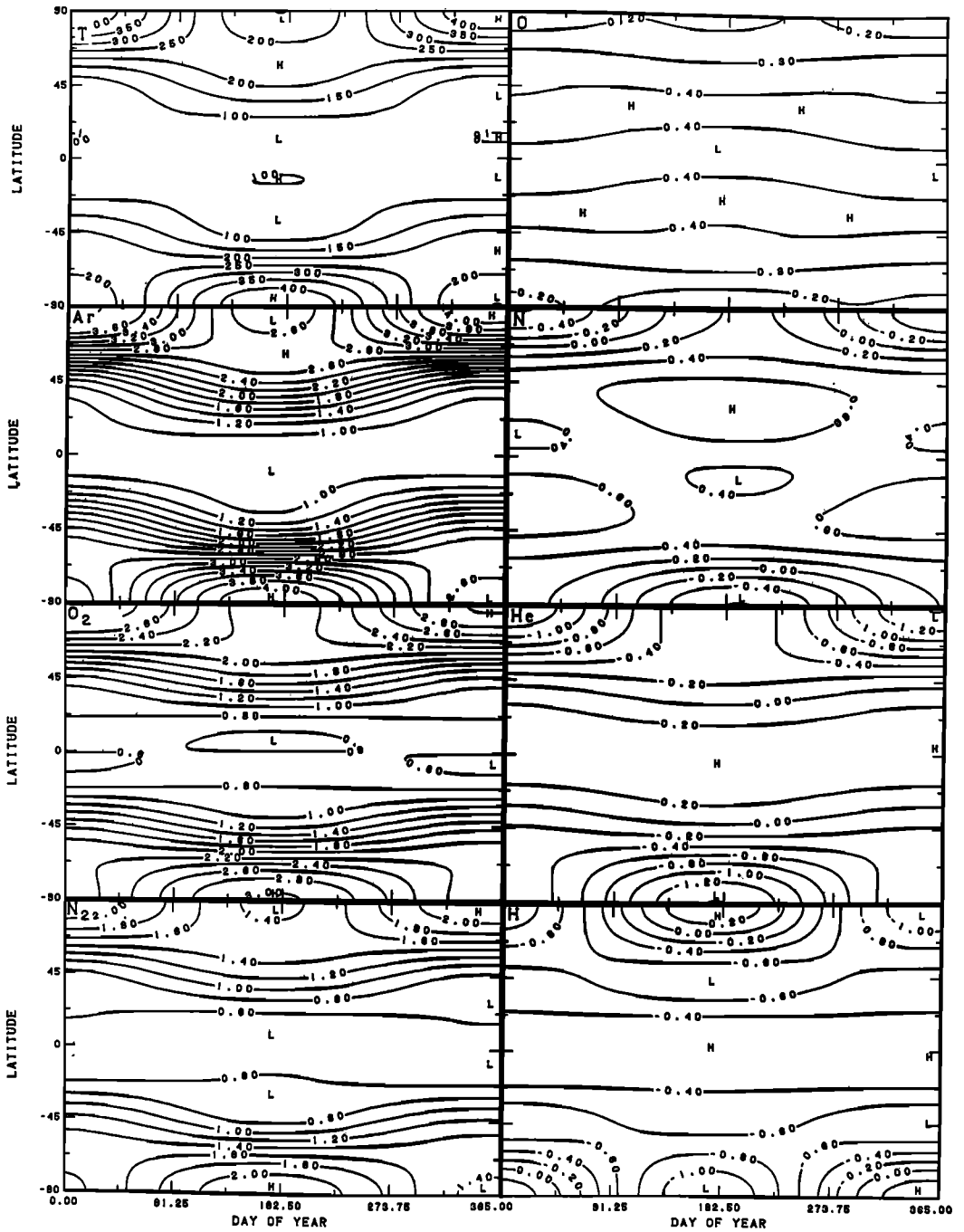

Fig. 5. Contour plot in latitude and day of year coordinates of temperature and natural logarithm of Ar, O_2, N_2, O, N, He, and H density differences between the MSIS-86 model with an Ap of 100 and the model with an Ap of 4 at 400 km for an $F_{10.7}$ of 150.

$$n(z, M) = (n_d(z, M)^A + n_m(z, M)^A]^{1/A} \cdot C_1(z)\ldots C_n(z) \quad \text{(A12a)}$$

$$A = M_h/(\bar{M}_o - M) \quad \text{(A12b)}$$

where

n ambient density, m^{-3};
n_d diffusive profile;
n_m mixing profile;
$M_h = 28$;
$\bar{M}_o = 28.95$;
M^o molecular weight of gas species.

The diffusive profile is

$$n_d(z, M) = n_\ell D(z, M)[T(z_\ell)/T(z)]^{1+\alpha} \quad \text{(A13)}$$

$$D(z, M) = D_B(z, M) \quad z \geq z_a \quad \text{(A14a)}$$

$$D(z, M) = D_B (z_a, M)$$

$$\cdot \exp \{\gamma_1[(x-1)/T_o + T_B (x^3 - 1)/3$$

$$+ T_C (x^5 - 1)/5 + T_D (x^7 - 1)/7]\} \quad z < z_a \quad \text{(A14b)}$$

$$D_B (z, M) = (T (z_\ell)/T(z)]^{\gamma 2}$$

$$\cdot \exp[-\alpha \gamma_2 \xi (z, z_\ell)] \quad \text{(A15)}$$

$$\gamma_2 = M g_\ell/(\sigma R_g T_\infty) \quad \text{(A16a)}$$

$$\gamma_1 = M g_a \xi (z_o, z_a)/R_g \quad \text{(A16b)}$$

$$g_\ell = g_s/(1 + z_\ell/R_p)^2 \quad \text{(A17a)}$$

$$g_a = g_s (1 + z_a/R_p)^2 \quad \text{(A17b)}$$

$$n_\ell = \bar{n}_\ell \exp [G(L)] \quad \text{(A18)}$$

where $\bar{n}_\ell$ is the average density at z_ℓ (fitting parameter) per cubic centimeter, g_s = 9.80665 x 10^{-3} km/s^2, R_g = 8.314 x 10^{-3} g km^2/mols s^2 - deg, α is the thermal diffusion coefficient, -0.4 for He and H, and zero otherwise.

The mixing profile with turbopause at z_h is

$$n_m (z, M) = n_\ell [D (z_h, M)/D (z_h, \bar{M}_o)]$$

$$\cdot [T(z_\ell)/T(z_h)]^\alpha D(z, \bar{M}_o) [T(z_\ell)/T(z)] \quad \text{(A19)}$$

Simulation of chemistry and dynamic flow effects to produce an effective turbopause which provides a specified mixing ratio to N_2 is as follows:

$$C_1 (z) = \exp \{R_1/[1 + \exp (z-z_1)/H_1]\} \quad \text{(A20a)}$$

$$R_1 = \log_e [\Omega n_m (z_\ell, 28)/n_m (z_\ell, M)] \quad \text{(A20b)}$$

where Ω is the mixing ratio relative to N_2 (fitting parameter for O, N and H), z_1 is the altitude at which log C_1 is R/2 (fitting parameter), and H_1 is the scale height for this correction (fitting parameter).

For O, N and H the above mixing ratio is conceived as that occurring without the loss/flow processes that produce the lower thermosphere peak. The peak is generated by a second factor:

$$C_2(z) = \exp \{R_2/[1 + \exp (z - z_2)/H_2]\} \quad \text{(A21)}$$

where R_2 is the density correction parameter (fitting parameter); z_2 is the altitude where log density correction is $R_2/2$ (fitting parameter), and H_2 is the scale height of this correction in kilometers (fitting parameter).

Expansion function for model quantities is as follows:

Time independent

$$G = a_{10} P_{10} + a_{20} P_{20} + a_{40} P_{40}$$

Solar activity

$$+ F_{00}^{a1} \Delta\bar{F} + F_{00}^{a2} (\Delta\bar{F})^2 + f_{00}^{a1} \Delta F$$

$$+ f_{00}^{a2} (\Delta F)^2 + \bar{f}_{20}^{a1} P_{20} \Delta\bar{F}$$

Symmetrical annual

$$+ c_{00}^{1} \cos \Omega_d(t_d - t_{00}^{c1})$$

Symmetrical semiannual

$$+ (c_{00}^{2} + c_{20}^{2} P_{20}) \cos 2 \Omega_d (t_d - t_{00}^{c2})$$

Asymmetrical annual (seasonal)

$$+ (c_{10}^{1} P_{10} + c_{30}^{1} P_{30}) F_1 \cos \Omega_d(t_d - t_{10}^{c1})$$

Asymmetrical semiannual

$$+ c_{10}^{2} P_{10} \cos 2 \Omega_d (t_d - t_{10}^{c2})$$

Diurnal

$$+ [a_{11} P_{11} + a_{31} P_{31} + a_{51} P_{51} + c_{21}^{1} P_{21}$$

$$\cdot \cos \Omega_d (t_d - t_{10}^{c1})] F_2 \cos \omega\tau$$

$$+ [b_{11} P_{11} + b_{31} P_{31} + b_{51} P_{51} + d_{21}^{1} P_{21}$$

$$\cdot \cos \Omega_d (t_d - t_{10}^{c1})] F_2 \sin \omega\tau$$

Semidiurnal

$$+ [a_{22} P_{22} + a_{42} P_{42} + (c_{32}^{1} P_{32} + c_{52}^{1} P_{52})\cos \Omega_d$$

$$\cdot (t_d - t_{10}^{c1})] \cdot F_2 \cos 2\omega\tau + [b_{22} P_{22}$$

$$+ b_{42} P_{42} + (d_{32}^{1} P_{32} + d_{52}^{1} P_{52})$$

$$\cdot \cos \Omega_d (t_d - t_{10}^{c1})] F_2 \sin 2\omega\tau$$

Terdiurnal

$$+ [a_{33} P_{33} + (c_{43}^{1} P_{43} + c_{63}^{1} P_{63})$$

$$\cdot \cos \Omega_d (t_d - t_{10}^{c1})]$$

$$\cdot F_2 \cos 3\omega\tau + [b_{33} P_{33} + (d_{43}^{1} P_{43} + d_{63}^{1} P_{63})$$

$$\cdot \cos \Omega_d (t_d - t_{10}^{c1})] F_2 \sin 3\omega\tau$$

Magnetic activity

$$+ [k_{00}^{a} + k_{20}^{a} P_{20} + k_{40}^{a} P_{40}$$

$$+ (k_{10}^{c1} P_{10} + k_{30}^{c1} P_{30} + k_{50}^{c1} P_{50})$$

$$\cdot \cos \Omega_d (t_d - t_{10}^{c1})$$

$$+ (k_{11}^{a} P_{11} + k_{31}^{a} P_{31} + k_{51}^{a} P_{51})$$

$$\cdot \cos \omega(\tau - t_{11}^{k})] \Delta A$$

Longitudinal

$$+ [a_{21}^{0} P_{21} + a_{41}^{0} P_{41} + a_{61}^{0} P_{61}$$

$$+ a_{11}^{0} P_{11} + a_{31}^{0} P_{31} + a_{51}^{0} P_{51}$$

$$+ (a_{11}^{c1} P_{11} + a_{31}^{c1} P_{31}) \cos \Omega_d (t_d - t_{10}^{c1})]$$

$$\cdot (1 + F_{21}^{a0} \Delta\bar{F}) \cos \lambda$$

$$+ (b_{21}^{0} P_{21} + b_{41}^{0} P_{41} + b_{61}^{0} P_{61})$$

$$+ b_{11}^{0} P_{11} + b_{31}^{0} P_{31} + b_{51}^{0} P_{51}$$
$$+ (b_{11}^{c1} P_{11} + b_{31}^{c1} P_{31}) \cos \Omega_d (t_d - t_{10}^{c1})]$$
$$\cdot (1 + F_{21}^{a0} \Delta\bar{F}) \sin \lambda$$

UT

$$+ (a_{10}^{1} P_{10} + a_{30}^{1} P_{30} + a_{50}^{1} P_{50})$$
$$\cdot (1 + F_{10}^{a1} \Delta\bar{F}) (1 + r_{10}^{a1} P_{10})$$
$$\cdot (1 + r_{10}^{c1} \cos \Omega_d (t_d - t_{10}^{c1}))$$
$$\cdot \cos \omega' (t - t_{10}^{a1})$$
$$+ (a_{32}^{1} P_{32} + a_{52}^{1} P_{52}) \cos [\omega'(t - t_{32}^{a1}) + 2\lambda]$$

UT/longitude/magnetic activity

$$+ (k_{21}^{a0} P_{21} + k_{41}^{a0} P_{41} + k_{61}^{a0} P_{61})$$
$$\cdot (1 + r_{21}^{k0} P_{10}) \Delta A \cos (\lambda - \lambda_{21}^{k0})$$
$$+ k_{11}^{c1} P_{11} \cos \Omega_d (t_d - t_{10}^{c1}) \Delta A$$
$$\cdot \cos (\lambda - \lambda_{11}^{kc})$$
$$+ [k_{10}^{a1} P_{10} + k_{30}^{a1} P_{30} + k_{50}^{a1} P_{50}] \Delta A$$
$$\cdot \cos \omega' (t - t_{10}^{k1}) \quad \text{(A22a)}$$

$$F_1 = 1 + F_{10}^{c} \Delta\bar{F} + f_{00}^{a1} \Delta F + f_{00}^{a2} (\Delta F)^2 \quad \text{(A22b)}$$

$$F_2 = 1 + F_{11}^{a} \Delta\bar{F} + f_{00}^{a1} \Delta F + f_{00}^{a2} (\Delta F)^2 \quad \text{(A22c)}$$

where $\Delta F = F_{10.7} - \bar{F}_{10.7}$, $\Delta\bar{F} = \bar{F}_{10.7} - 150$, $F_{10.7}$ = 10.7 cm flux on previous day, 10^{-22} W m^{-2} Hz^{-1}, $\bar{F}_{10.7}$ is the average $F_{10.7}$ over three solar rotations (81 days) centered on required day, P_{nm} are the nonnormalized Legendre-associated functions, equal to $[(1-x^2)^{m/2}/2^n\, n!]$ $(d^{n+m}/dx^{n+m})\ (x^2 - 1)^n$, with $x = \cos\theta$ and θ = geographic latitude, $\Omega_d = 2\pi/365$ day^{-1}, $\omega = 2\pi/24$ h^{-1}, $\omega' = 2\pi/86400$ s^{-1}, τ is local time in hours, t is UT in seconds, t_d is the day count in year, and λ is geographic longitude (eastward positive).

The magnetic activity factor is to be chosen from either

$$\Delta A = (Ap - 4) + (k_{00}^{r} - 1) \{Ap - 4$$
$$+ [\exp (-k_{00}^{s} (Ap - 4)) - 1]/k_{00}^{s}\} \quad \text{(A23)}$$

where Ap is the daily magnetic index or

$$\Delta A = \{g (a_1) + [g (a_2) E(\beta) + g (a_3) E(\beta)^2$$
$$+ g (a_4) E(\beta)^3 + (g (\bar{a}_{12}) E(\beta)^4 + g(\bar{a}_{30}) E(\beta)^{12}$$
$$\cdot (1 - E(\beta)^8)/(1 - E (\beta))]\}/\Sigma(\beta) \quad \text{(A24a)}$$

$$E(\beta) = \exp (-10800\, \beta) \quad \text{(A24b)}$$

$$\Sigma(\beta) = 1 + (1 - E(\beta)^{19})$$
$$\cdot E (\beta)^{(0.5)}/(1 - E(\beta)) \quad \text{(A24c)}$$

$$g(a) = (a - 4) + (k_{00}^{r} - 1) \{a - 4$$
$$+ [\exp (-k_{00}^{s} (a - 4)) - 1]/k_{00}^{s}\} \quad \text{(A24d)}$$

$$\beta = \beta_{00}/[1 + \beta_{10} (45 - |\theta|)] \quad \text{(A24e)}$$

where β is the inverse of time constant for magnetic activity effect per second, $t_m = t \pmod{10800}$, a_1, a_2, a_3, a_4 are the 3-hour Ap index for current time and 3, 6, and 9 hours before current time, a_{12} is the average of eight 3-hour Ap indices from 12 to 35 hours prior to current time, and a_{36} is the average of eight 3-hour Ap indices from 36 to 59 hours prior to current time.

Acknowledgments. In addition to all the people who helped make available the data for the MSIS-83 model, the author would like to thank M. J. Engebretson for making available atomic nitrogen data from the AE and DE satellites, N. W. Spencer and L. E. Wharton for making available preliminary DE temperature data, and D. Alcayde for sending the latest St. Santin temperature data.

The Editor thanks D. W. Rusch and two other referees for their assistance in evaluating this paper.

References

Carignan, G. R., B. P. Block, J. C. Maurer, A. E. Hedin, C. A. Reber, and N. W. Spencer, The neutral mass spectrometer on Dynamics Explorer, Space Sci. Instrum., 5, 429-441, 1981.

Engebretson, M. J., and K. Mauersberger, The response of thermospheric atomic nitrogen to magnetic storms, J. Geophys. Res., 88, 6331-6338, 1983.

Engebretson, M. J., and J. T. Nelson, Atomic nitrogen densities near the polar cusp, J. Geophys. Res., 90, 8407-8416, 1985.

Engebretson, M. J., K. Mauersberger, D. C. Kayser, W. E. Potter, and A. O. Nier, Empirical model of atomic nitrogen in the upper thermosphere, J. Geophys. Res., 82, 461-471, 1977.

Engebretson, M. J., J. A. DeFreese, and K. Mauersberger, Diurnal, seasonal, and nighttime variations of atomic nitrogen in the equatorial thermosphere, J. Geophys. Res., 85, 2165-2170, 1980.

Gerard, J.-C., R. G. Roble, D. W. Rusch, and A. I. Stewart, The global distribution of thermospheric odd nitrogen for solstice conditions during solar cycle minimum, J. Geophys. Res., 89, 1725-1738, 1984.

Hays, P. B., T. L. Killeen, and B. C. Kennedy, The Fabry-Perot interferometer on Dynamics Explorer, Space Sci. Instrum., 5, 395-416, 1981.

Hedin, A. E., A revised thermospheric model based on mass spectrometer and incoherent scatter data: MSIS-83, J. Geophys. Res., 88, 10,170-10,188, 1983.

Hedin, A. E., and G. R. Carignan, Morphology of thermospheric composition variations in the quiet polar thermosphere from Dynamics Explorer measurements, J. Geophys. Res., 90, 5269-5277, 1985.

Hedin, A. E., and M. J. Engebretson, Empirical model of thermospheric atomic nitrogen, Eos Trans. AGU, 67, 322, 1986.

Hedin, A. E., C. A. Reber, N. W. Spencer, H. C. Brinton, and D. C. Kayser, Global model of longitude/UT variations in thermospheric composition and temperature based on mass spectrometer data, J. Geophys. Res., 84, 1-9, 1979.

Hernandez, G., Mid-latitude thermospheric neutral kinetic temperatures, 1, Solar geomagnetic and long term effects, J. Geophys. Res., 87, 1623-1632, 1982.

Jacchia, L. G., Thermospheric temperature, density, and composition: New models, Spec. Rep., 375, Smithson. Astrophys. Observ., Cambridge, Mass., 1977.

Kohnlein, W., D. Krankowsky, P. Lammerzahl, W. Joos, and H. Volland, A thermospheric model of the annual variations of He, N, O, N_2, and Ar from the AEROS NIMS data, J. Geophys. Res., 84, 4355-4362, 1979.

Mauersberger, K., M. J. Engebretson, W. E. Potter, D. C. Kayser, and A. O. Nier, Atomic nitrogen measurements in the upper atmosphere, Geophys. Res. Lett., 2, 337-340, 1975.

Oliver, W. L., Incoherent scatter radar studies of the daytime thermosphere, Ann. Geophys., 35, 121-139, 1979.

Oliver, W. L., Improved Millstone Hill exospheric temperature measurements: Evidence for a seasonal variation of the magnetic activity effect, J. Geophys. Res., 85, 4237-4247, 1980.

Sharp, L. R., D. R. Hickman, C. J. Rice, and J. M. Straus, The altitude dependence of the local time variation of thermospheric density, Geophys. Res. Lett., 5, 261-263, 1978.

Spencer, N. W., L. E. Wharton, H. B. Niemann, A. E. Hedin, G. R. Carignan, and J. C. Maurer, The Dynamics Explorer wind and temperature spectrometer, Space Sci. Instrum., 5, 417-428, 1981.

Wand, R. H., Lower thermospheric structure from Millstone Hill incoherent scatter radar measurements, 1, Daily mean temperature, J. Geophys. Res., 88, 7201-7209, 1983a.

Wand, R. H., Lower thermospheric structure from Millstone Hill incoherent scatter radar measurements, 2, Semidiurnal temperature component, J. Geophys. Res., 88, 7211-7224, 1983b.

A. E. Hedin, Planetary Atmospheres Branch, Code 614, NASA Goddard Space Flight Center, Greenbelt, MD 20771.

(Received August 22, 1986;
revised October 27, 1986;
accepted January 7, 1987.)